Tujunen, Noora; Kaivosoja, Emilia; Protopopova, Vera; Valle-Delgado, Juan José; Österberg, Monika; Koskinen, Jari; Laurila, Tomi

Electrochemical detection of hydrogen peroxide on platinum-containing tetrahedral amorphous carbon sensors and evaluation of their biofouling properties

Published in:
Materials Science and Engineering C: Materials for Biological Applications

DOI:
10.1016/j.msec.2015.05.060

Published: 01/10/2015

Document Version
Peer-reviewed accepted author manuscript, also known as Final accepted manuscript or Post-print

Please cite the original version:
Tujunen, N., Kaivosoja, E., Protopopova, V., Valle-Delgado, J. J., Österberg, M., Koskinen, J., & Laurila, T. (2015). Electrochemical detection of hydrogen peroxide on platinum-containing tetrahedral amorphous carbon sensors and evaluation of their biofouling properties. *Materials Science and Engineering C: Materials for Biological Applications*, *55*, 70-78. https://doi.org/10.1016/j.msec.2015.05.060

Electrochemical detection of hydrogen peroxide on platinum-containing tetrahedral amorphous carbon sensors and evaluation of their biofouling properties

Noora Tujunen[a], Emilia Kaivosoja[a], Vera Protopopova[b], Juan José Valle-Delgado[c], Monika Österberg[c], Jari Koskinen[b], Tomi Laurila[a] *

[a] Department of Electrical Engineering and Automation, School of Electrical Engineering, Aalto University, PO Box 13500, 00076 Aalto, Finland

[b] Department of Materials Science and Engineering, School of Chemical Technology, Aalto University, PO Box 16200, 00076 Aalto, Finland

[c] Department of Forest Products Technology, School of Chemical Technology, Aalto University, Finland, PO Box 16300, 00076 Aalto, Finland

*Corresponding author: tomi.laurila@aalto.fi, +358 50 341 4375

Abstract

Hydrogen peroxide is the product of various enzymatic reactions, and is thus typically utilized as the analyte in biosensors. However, its detection with conventional materials, such as noble metals or glassy carbon, is often hindered by slow kinetics and biofouling of the electrode. In this study electrochemical properties and suitability to peroxide detection as well as ability to resist biofouling of Pt-doped ta-C samples were evaluated. Pure ta-C and pure Pt were used as references. According to the results presented here it is proposed that combining ta-C with Pt results in good electrocatalytic activity towards H_2O_2 oxidation with better tolerance towards aqueous environment mimicking physiological conditions compared to pure Pt. In biofouling experiments, however, both the hybrid material and Pt were almost completely blocked after immersion in protein-containing solutions and did not produce any peaks for ferrocenemethanol oxidation or reduction. On the contrary, it was still possible to obtain clear peaks for H_2O_2 oxidation with them after similar treatment. Moreover, quartz crystal microbalance experiment showed less protein adsorption on the hybrid sample compared to Pt which is also supported by the electrochemical biofouling experiments for H_2O_2 detection.

Keywords: tetrahedral amorphous carbon, platinum, hydrogen peroxide, sensor, biofouling

1. Introduction

Hydrogen peroxide (H_2O_2) is simple molecule that has widespread usage ranging from industry and food to clinical applications. It has high standard electrochemical potential [1] which makes it a powerful oxidizing agent. It can be either electrochemically oxidized to O_2 ($E^0 = 0.695$ V) or reduced to water ($E^0 = 1.763$ V) in diffusion controlled two-electron processes [2]. In industrial applications H_2O_2 and its redox reactions are closely linked to fuel cell technology as it has been proposed to be formed as reaction intermediate in the oxygen reduction reaction [2], [3]. In living organisms cells produce H_2O_2 mitochondria to control growth and apoptosis. It has also been suggested that H_2O_2 has a key role in aging [4]. Furthermore, it is formed as a by-product in various enzymatic reactions, such as those catalyzed by glucose oxidase [5], glutamate oxidase [6], and cholesterol oxidase [7]. Enzymatic production makes H_2O_2 feasible for biosensor applications as it typically has lower oxidation potential compared to the enzyme substrate molecules.

Carbon-based materials are often considered as good candidates in sensor applications owing to their low cost, wide potential window, relative electrochemical inertness and adequate electrocatalytic activity in various redox reactions [8]. However, in detecting H_2O_2 carbon materials as such do not typically perform as well as noble metals, for instance Au and Pt [9]. It has been shown that pure glassy carbon does not catalyze redox reactions of H_2O_2 but by modifying the electrode surface for example with Ag [10]–[12], Pd [13], [14], Pt [15] or carbon nanotubes [16] can result in measurable electrochemical reactions. In addition, Hrapovic *et al.* [15] demonstrated with their glassy carbon and carbon nanotube sensors that the detection limit for H_2O_2 with Pt-doped sensors strongly depends on the type of the carbon support.

Despite their good catalytic activity towards electrochemical oxidation and reduction of H_2O_2, the disadvantages of noble metals, especially Pt, include high cost and susceptibility to biofouling. Expenses can be lowered by using nanomaterials which also typically increases the surface area and can also increase the number of active sites [17]. Biofouling has been proposed as the main reason for biosensor failure *in vivo* [18]. It can be characterized as accumulation of undesired biological material, such as proteins and cells, on sensor surface [18], [19]. It is detrimental to the sensor function as it may prevent the necessary contact between the analyte and the surface.

Moreover, the detection of H_2O_2 on conventional metal or carbon fiber electrodes is hindered by slow kinetics [10], [20] and relatively high overpotential [21], which allows also the oxidation of interfering species, such as ascorbic acid and uric acid [10]. Thus, new materials that facilitate fast and interference-free detection of H_2O_2 as well as resist biofouling are in demand.

Tetrahedral amorphous carbon (ta-C) is hydrogen-free and consequently the hardest, strongest, and slickest form of diamond-like carbon (DLC). In addition, DLC has previously been shown to resist microbial and protein attachment [22] which indicates that ta-C also could possess similar antifouling properties. On the other hand, adsorption of bovine albumin serum (BSA) is suggested to be favored on ta-C when compared to other types of DLC with higher hydrogen content and lower sp^3 fraction [23]. With its large water window (3.7 V in H_2SO_4 and 3 V in PBS [24]) ta-C is a feasible material for electrochemical detection of various analytes in aqueous media [25]. However, in our experience pure ta-C surfaces typically perform poorly in detecting H_2O_2. In order to overcome this we have doped our ta-C samples with Pt in order to enhance the oxidation of H_2O_2. To our knowledge, no Pt-doped ta-C has been fabricated and used in electrochemical detection of H_2O_2 before. However, it has been shown that doping DLC with Pt affect its electrochemical properties [26]–[28]. Pleskov *et al.* [28] suggested that Pt acts as a catalyst for charge transfer in otherwise electrochemically inactive DLC. On the contrary, our ta-C is innately electrochemically active and adding Pt is aimed at oxidation of H_2O_2. Moreover, we have previously shown that functionalizing ta-C with NH_2 groups allows the immobilization of GluOx on ta-C [29] which makes the material suitable candidate for biosensor applications. In addition, our ta-C electrodes with small exposed Pt areas were an order of magnitude more sensitive towards dopamine compared to Pt electrodes [30], [31]. In this paper we inspect detection of H_2O_2 on hybrid Pt-doped ta-C in comparison with pure ta-C and Pt and evaluate biofouling properties of the samples by immersion in protein solutions.

2. Materials and Methods

2.1. Sample fabrication

Studied samples consisted of 20 nm thick underlying titanium layer and 7 nm thick undoped or Pt-doped ta-C layer with Pt atomic concentration of 0 and 20%. Samples with 8 nm thick Pt layer only were fabricated as well. Substrates were either highly conductive p-type boron-doped (100) Si wafers with 0.001–0.002 Ω-cm resistivity (Ultrasil, USA) or silica-coated quartz crystals (Q-Sense, Biolin Scientific, Sweden) designed for quartz crystal microbalance with dissipation (QCM-D) experiments. Silicon wafers were cleaned by standard RCA-cleaning procedure before deposition.

Sample fabrication procedure consisted of direct current magnetron sputtering (DC-MS) for Ti layer and dual filtered cathodic vacuum arc (FCVA) deposition for carbon and platinum layers. Both deposition systems were installed in one chamber. DC-MS system was equipped with a circular and water-cooled magnetron sputtering source with 2 inch Ti target. Titanium underlying layers were deposited under the following deposition conditions: discharge power was fixed at 100 W, total pressure was 0.67 Pa, Ar gas flow rate was 28 sccm, deposition temperature was close to room temperature, and deposition time was 350 s. Cathodic arc deposition system (Lawrence Berkeley National Laboratory, USA) was equipped with a 60^o bent magnetic filter for reduction of macroparticle contamination. In order to obtain Pt-doped ta-C, composite cathode made of 6.35 mm graphite rod and two embedded 1 mm Pt wires in the center were used. For deposition of ta-C or Pt layers only, separate graphite and platinum cathodes were utilized. The arc current pulses had amplitude of 0.7 kA and 0.6 ms pulse width. Each pulse was triggered at 1 Hz frequency. The 2.6 mF capacitor bank was charged to 400 V. Number of pulses was 360 for carbon and combined cathodes and 1440 for Pt. Total pressure during the deposition process was no less than $1.3 \cdot 10^{-4}$ Pa. The distance between the substrate holder and the filter was about 20 cm. Samples were placed in the rotating holder (rotational velocity used was 20 rpm).

After deposition wafers were cut into rectangular chips with an automated dicing saw. Samples were stored dry in room temperature. Before electrochemical characterization and biofouling experiments circular area (0.28 cm^2 or 0.50 cm^2) was defined from the sample with PTFE tape (Irpola Oy, Finland) or with custom made polycarbonate sample holder.

2.2. Physical characterization of samples

The sample morphology was studied with optical microscopy (Leica DMRX, Leica Microsystems, Germany), scanning electron microscopy (SEM, Hitachi-4700, Hitachi Ltd, Japan) and scanning probe microscopy (Ntegra Aura, NT-MDT Company, Russia). The latter, operated in ambient atmosphere with variable measuring facilities, was used for atomic force microscopy (AFM) and spreading resistance microscopy, i.e. conductive-AFM (c-AFM) and current-voltage spectroscopy. The measurements were carried out in ‘scanning by sample’ mode. For c-AFM, a diamond coated conductive probe (DCP10 or HA_HP_DCP, NT-MDT Company, Russia) was mounted on a special probe holder designed for the current measurements under the varied voltage applied to the probe. The measurements were performed in contact regime. The typical curvature radius of a tip was about 100 nm. The force constant values are nominally 11.5 N/m and 16±3.2 N/m for DCP10 and HA_HP_DCP cantilevers, respectively. Bitmap images (topography and current maps) were processed with Gwyddion (version 2.34) software.

In order to define Pt atomic concentration of the hybrid sample, X-ray fluorescence (XRF) spectroscopy (Spectroscan MAX-GV, Spectron Ltd, Russia) was utilized. Quantitative analysis was made according to a calibration curve. Dependence of Pt atom number on intensity of Pt characteristic line (1312.6 Å for LiF200 detector) was determined for samples consisting of single platinum layers with different thicknesses deposited on Si wafer. Thickness was used as a measure of number of Pt atoms. The real thickness of Pt layers was measured with a Dektac XT profilometer (Bruker Corporation, USA) with 6 Å step height repeatability.

Samples containing ta-C were characterized with visible Raman spectroscopy (WITec alpha 300 spectrometer, **WITec Wissenschaftliche Instrumente und Technologie GmbH, Germany**). Spectra were acquired with 532 nm laser wave length and 0.5 s exposure time. All obtained spectra were processed by averaging of 50 spectra and a background subtraction. Non-linear spectrum background was caused by silicon signal masked partly by Ti and ta-C layers. In order to make accurate fitting of carbon peaks (Gaussian function), reduced Si spectra was subtracted. It is to be noted, that Raman spectrum of ta-C typically shows a D-band peak (~1360 cm^{-1}) and a G-band peak (~1560 cm^{-1}) [35], [36]. Their ratio I(D)/I(G) is correlated to the sp^3/sp^2 fraction ratio, the band gap value, and film density.

2.3. Electrochemical measurements

Cyclic voltammetry was performed with a Gamry Reference 600 potentiostat and Gamry Framework software (Gamry Instruments, USA). Reference electrode was a skinny Ag/AgCl electrode (Sarissa Biomedical Ltd, U.K.) and counter electrode a glassy carbon rod.

In order to clean the samples they were cycled in nitrogen purged 0.15 M H_2SO_4 for at least 100 cycles between -0.4 V and 1.3 V vs. Ag/AgCl with 1 V s^{-1}. H_2O_2 solutions (0 – 100 mM) were freshly prepared from 30 % H_2O_2 (Merck KGaA, Germany) by dilution in phosphate buffered saline (PBS, pH 7.4). The experiments were conducted by immersing the sample in nitrogen purged H_2O_2 solutions and cycling 3 times between -0.4 V and 1.3 V vs. Ag/AgCl with cycling rate of 50 mV s^{-1}.

2.4. Biofouling

Biofouling of the samples was investigated based on the protocol described by Goto *et al.* [19]. Briefly, the samples were first cleaned electrochemically as described in previous section and their response to nitrogen purged 1 mM ferrocenemethanol (FcMeOH, Sigma-Aldrich Co., USA) in 0.15 M H_2SO_4 or PBS between -0.4 V and 0.3 V vs. Ag/AgCl or between -0.3V and 0.5 V, respectively, was measured with cycling rate of 400 mV s^{-1}. Next, the samples were immersed either in 10 mg/ml of bovine serum albumin (BSA, Amresco LLC, USA) in deionized water or pure deionized water. After 24h incubation at room temperature the experiment in FcMeOH was repeated.

2.5.Quartz crystal microbalance with dissipation monitoring (QCM-D)

The adsorption of BSA on different substrates was studied with QCM-D using a Q-Sense E4 instrument (Q-Sense, Sweden). BSA was dissolved in PBS to 1 g l^{-1} concentration and syringe filtered through 0.45 µm filter. Each experiment was performed at 37 °C and 0.1 ml min^{-1} flow rate. Analysis of the results was carried out by utilizing the Sauerbrey equation [32] which states that the change in resonance frequency ($\Delta \boldsymbol{f}$) of the quartz crystal sensor is proportional to the mass adsorbed per unit surface ($\Delta \boldsymbol{m}$):

$$\Delta m = -C\Delta f/n,$$

where $\boldsymbol{C}$ is the sensitivity constant (here $\boldsymbol{C} = 0.177$ mg/m^2 Hz) and $\boldsymbol{n}$ is the overtone number (here $\boldsymbol{n} = 3$).

3. Results and discussion

3.1. Physical characterization of samples

The results from the optical microscopy together with SEM demonstrated that all samples had, in average, quite uniform topography without any significant structural features (images not shown here). This was further confirmed with atomic force microscopy. Topography maps for ta-C and Pt-doped ta-C (ta-C/Pt) are presented in Figure 1 (top row). The values of average roughness are in the range of 1.15±0.14, 1.08±0.28 and 0.43±0.11 nm for ta-C, ta-C/Pt and Pt samples, respectively (Table 1). The former, larger values for ta-C and ta-C/Pt derive from the fact that ta-C follows the topography of the underlying Ti layer as shown in [24]. Ti layer is used here as an adhesion promoter for undoped and Pt-doped ta-C. The XRF compositional analysis (Table 1) demonstrates that Pt-doped sample contains approximately 20 at. % of Pt.

C-AFM measurements show that the average current flowing through the ta-C/Pt sample was larger in comparison to that of ta-C, as determined with two different types of probes and with two different applied bias voltage values. The average current through the sample with Pt layer was one magnitude higher in comparison to ta-C samples even when only tenth of the bias voltage was used (Table 1). The probes had different original specifications, and thus, before actual measurements force-distance spectroscopy was carried out in order to find the actual value of passing force between the probe and the sample surface. Passing force values were 2.1 and 0.75 µN for DCP10 and HA_HP_DCP probes, respectively [31]. Current maps are presented in Figure 1 (for HA_HP_DCP probe only). A particular feature of current maps is the non-uniform distribution of current. Higher current regions are correlated to the valleys, whereas the smaller current areas correlate with the hills on the surface. This non-uniformity can be connected with different mechanical contacts established between the probe and the real rough surface [33]. Mechanical properties of the contact can be described with the use of Hertz elastic contact theory [33]–[35] and ball-ball approximation. Our estimations [36] made for the real geometry (the probe radius of 100 nm, the width and the height of the each surface grain are 150 and 1 nm) show that, if the probe is in the contact with the grain top or the lateral surface of the grain, the contact radius values are 7.5 nm and 5.3 and the contact area values are 177 nm^2 and 88 nm^2 for DCP10 and HA_HP_DCP probes, respectively. However, if the probe is located in the valley and in the contact with two adjacent grains, the contact radius and the contact area are twice as big. Spreading resistance values were found from the equation for voltage between the probe with hemisphere shape and the collecting contact of certain radius. Consequently, the values decrease from $8.9 \cdot 10^3$ Ω cm for ta-C to $2.5 \cdot 10^3$ Ω cm for ta-C/Pt and 15.6 Ω cm for Pt (Table 1).

In addition, current-voltage spectroscopy (Figure 2) demonstrated that electrical conduction mechanism through both ta-C containing samples can be described in terms of space-charge-limited (SCL) currents theory [24], [37], [38] with the presence of several levels of monoenergetic traps. Thus, current-voltage curves plotted in log-log coordinates (Figure 2b) contain Ohm’s law regions (slope is one) and several regions with the slope equaled to two, which relate to presence of traps. It should be noted that while in case of Pt layer on top of silicon conduction mechanism is expressed as Ohm’s law it is also possible that Schottky contact is established [39] between Si and Pt.

The results from Raman spectroscopy are presented in Figure 3. No smoothing was applied and the spectrum shown in Figure 3 is the original with subtracted background only. Total intensity of ta-C spectra decrease and I(D)/I(G) ratio increase with addition of Pt. It is possible that is caused by higher sp^2 fraction in the Pt containing films, consistent with the results in [40], as higher value of I(D)/I(G) ratio is typically associated with higher sp^2 content [41]–[43]. In addition, it was suggested in [40] that metal doping could lead to conductive path formation in the film.

Thus, it is suggested that addition of Pt induces formation of higher amount of sp^2 fraction and higher conductivity for ta-C. Menegzzo *et al*. [26] have previously reported similar results for Pt containing DLC. Moreover, it was show here that adding Pt in ta-C does not significantly change conduction mechanism from SCL currents theory significantly. The conduction mechanism through Pt layer is defined by Ohm's law, as expected.

3.2.Electrochemical measurements

Voltammograms for ta-C, ta-C/Pt and Pt in 0.15 M H_2SO_4 are presented in Figure 4. Water window in H_2SO_4 and the double-layer capacitance have been previously determined for pure ta-C [24]. Pt sample exhibits typical Pt features with clear peaks for hydrogen adsorption and desorption as well as for Pt surface oxidation and reduction [44]. For ta-C/Pt it is suggested that the anodic peak at -0.48 V and cathodic peak at -0.46 V (inset in Figure 4) are also related to hydrogen adsorption and desorption, respectively, and indicate the presence of Pt in the material. Menegazzo *et al*. [26] inspected the electrochemical properties of Pt-DLC and Au-DLC films. They concluded that even though the working range for the composite is narrower compared to the carbon support alone it is still larger than for pure metal offering also chemical and mechanical stability of an inert ceramic. However, in our case the presence of Pt in the hybrid samples is more evident from the voltammograms compared to those presented by Menegazzo *et al*. Thus, it is concluded that even though the hybrid material would allow higher potentials at the anodic end, and thus also larger water window compared to pure Pt, it is recommended to work within the conventional potential range used for Pt to avoid any uncontrolled modifications of the surface.

The double-layer pseudocapacitance was determined from the CV curves in H_2SO_4 ($\Delta j = 2 \times C \times v$). The geometric area of the sample in contact with the solution was used in the calculations and the Δj was defined as the difference between anodic and cathodic current densities. For ta-C/Pt and Pt samples it is noted that as they have been cycled up to 1.3 V vs. Ag/AgCl during the cleaning step it is likely that there were some oxide species present on the surface even though the capacitance was determined from dataset where the cycling was not extended into the oxide formation region. Thus all the values in Table 2 correspond to pseudocapacitance as they probably include also some contribution from faradaic reactions [24], [45]. Especially, for Pt sample there were most likely considerable faradaic contributions that resulted in large error for the pseudocapacitance.

Cyclic voltammograms recorded with different concentrations of H_2O_2 are presented in Figure 5. Pure ta-C samples (Figure 5) show no peaks that would indicate oxidation or reduction of the analyte. However, hybrid sample as well as Pt samples showed clear peaks at approximately 0.6 V for concentrations of 1000 µM and 10 mM. The insets show that both ta-C/Pt and Pt samples were able to detect also 100 µM of H_2O_2. The peak positions and corresponding current densities for 1000 µM H_2O_2 are presented in Table 2. The current at the peak potential clearly increased with increasing concentration. In general, when compared to the Pt sample the hybrid sample as well as the pure ta-C show considerably smaller background current densities. Especially the O_2 evolution above 1 V typical of Pt in PBS is more limited on the hybrid samples reflecting instead the behavior of ta-C.

Hudak *et al*. [46] studied cyclic voltammograms of Pt recorded in PBS (pH 7.2). Although between -0.6 V and 0.9 V vs. Ag/AgCl the response was well in line with the standard H_2SO_4 curves often used in the study of Pt electrochemistry, in the extended potential range from -1.0 V to 1.7 V vs. Ag/AgCl Pt exhibited some additional electrochemical activity, especially above 1 V vs. Ag/AgCl and at approximately -0.75 V vs. Ag/AgCl. This was suggested to arise from oxidation of chloride ions and oxidation/reduction of phosphate ions [46]. Despite the narrower potential range similar reactions are proposed to occur on the surface of the Pt sample above 1.0 V vs. Ag/AgCl. These reactions are absent on the ta-C and hybrid sample indicating better tolerance for environment mimicking physiological conditions compared to pure Pt. Especially inhibition of H_2O_2 oxidation by chloride ions has been stated as one of the challenges associated with Pt electrodes [47]. The results presented here are proposed to indicate that it is possible to obtain good electrocatalytic activity for H_2O_2 oxidation with less interference from the ions in the electrolyte by combining Pt with ta-C. The optimal concentration of Pt in the hybrid samples that would allow detection of H_2O_2 in the low micromolar range as well still remains to be determined.

It has been shown by Sitta *et al*. [48] by studying H_2O_2 reactions on Pt single crystals that both its oxidation and reduction depend on the surface structure and oxygen coverage. It is therefore suggested that by controlling the Pt orientation in the hybrid samples one could improve sensitivity towards H_2O_2. This issue will be studied in detail in the near future.

3.3. Biofouling

The ability to resist biofouling is crucial for the successful operation of a biosensor. In order to study the biofouling properties of the samples they were immersed in BSA solutions for 24 hours at room temperature to compare the current responses for FcMeOH in H_2SO_4 or PBS before and after exposure to possibly fouling solutions. It has been previously shown that serum albumin adsorbs on Pt containing biosensor surface [49] which justifies the use of BSA as a model solution. Samples were also immersed in deionized water for reference. The isoelectric point of BSA is 4.7 [50] and that of ta-C is 2.6 [24] which indicates that the surface should in general repel the protein both in neutral pH as well as below pH 1. However, it should also be noted that protein absorption is a complex process and cannot be predicted based on a single parameter such as charging.

Results from the first set of experiments where H_2SO_4 was used as solvent are presented in Figure 6. Cycling in H_2SO_4 was used to clean the surfaces in order to evaluate if it was possible to recover the initial response to FcMeOH after immersion in BSA. It is evident, that all the samples were affected by immersion in BSA solution. For pure ta-C the peak separation increased from 75 mV to 130 mV and was not recovered to the initial value after cleaning as was the case with pure Pt. The hybrid sample was completely blocked by BSA and there was only minor recovery upon cleaning (Figure 6, no peak separation defined). Pt sample was also clearly fouled by BSA as the peak separation increased from 69 mV to 226 mV. However, after cleaning the peak separation was decreased back to 78 mV which is close to the original value. The difference between ta-C and ta-C/Pt should not arise from the difference in sp^3 content (Table 1) as it has been previously shown by Vinnichenko *et al*. [51] that it does not affect protein adsorption.

Moreover, both Pt containing samples (ta-C/Pt and Pt) were also affected by immersion in deionized water. For ta-C/Pt the peak separation was 20 mV lower than the value before immersion (Table 1). For Pt sample peak separation was increased only by 9 mV. However, the current density after immersion was significantly smaller than the initial value which is proposed to indicate a decrease in the active area or in the number of adsorption cites. This could arise for example from adsorption of impurities from the solution or excessive oxidation of Pt films.

The above experiments were conducted in acidic environment which may have resulted into an excessive denaturation of the protein on the electrode surface. Thus, in the second set FcMeOH was dissolved in PBS (pH ~7.4) in order to avoid unwanted changes in the protein. Results are presented in Figure 7. Similarly as when the experiment was conducted in acidic environment, immersion in BSA affected all the samples. For ta-C the peak separation increased from 76 mV to 136 mV which is comparable with the previous results for ta-C. Both ta-C/Pt and Pt were blocked by the protein and no clear peaks were obtained for FcMeOH oxidation and reduction. Immersion in deionized water did not noticeably affect either ta-C or ta-C/Pt which corresponds well with the previous experiments. However, Pt sample was significantly blocked also after incubation in deionized water.

Comparing Figure 6 and Figure 7 shows that both ta-C and ta-C/Pt behave in a fairly similar manner regardless of the solvent (H_2SO_4 or PBS, respectively). However, when PBS was utilized as solvent pure Pt lost activity for FcMeOH oxidation and reduction both after immersion in deionized water and immersion in BSA. Interestingly, this was not the case when FcMeOH was dissolved in H_2SO_4. Figure 6C shows clear peaks for FcMeOH both after incubating in deionized water and BSA. It is proposed that Pt surface is actually cleaned in H_2SO_4 based on the following arguments: (i) From the Pourbaix diagram of Pt it can be seen that the stability region of metallic Pt is higher at low pH (< 1) than at physiological pH and (ii) the results obtained upon purposely cleaning the sample by cycling in H_2SO_4 after immersion in BSA (blue dashed line in Figure 6) showing that the initial peak separation could be gradually recovered.

For ta-C it is mostly the protein that fouls the surface whereas for Pt there seem to be also other factors (not specified here) that result in losing the response to FcMeOH.

In addition, it is important that the sensors retain the ability to detect H_2O_2 even after exposure to possibly fouling solutions. Thus, similar experiments as done for the electrochemical characterization with H_2O_2 were conducted also after immersion in deionized water or BSA. Pure ta-C was omitted as it did not produce any peak for H_2O_2 (Figure 5). Results are presented in Figure 8. They indicate, on the contrary to the previous experiments, that neither Pt nor ta-C/Pt are completely blocked but retain their ability to detect H_2O_2 regardless of whether they have been immersed in deionized water or BSA. This could be a consequence of smaller size of H_2O_2 compared to FcMeOH utilized in previous experiments.

Figure 8 shows that the peak was more sharply defined for Pt than for ta-C/Pt. This is suggested to arise from the hybrid nature of the ta-C/Pt sample as the responses to H_2O_2 of pure ta-C and pure Pt (Figure 5) are mixed on it. There was no clear reduction peak visible for H_2O_2 and hence it was not possible to define peak separation. However, the changes in the peak intensity (current density) and position (potential) after immersions were evaluated for the response in 1 mM H_2O_2 solution. After immersion in deionized water the peak for ta-C/Pt was shifted by 20 mV in the negative direction whereas for Pt it was shifted only 5.8 mV in the positive direction. After immersion in BSA solution the peak position shifted in the positive direction for both samples. The shift was considerably larger for sample Pt (54.2 mV) compared to ta-C/Pt (44.2 mV).

Current densities were always smaller after than before immersion regardless of the sample or solution type. The change in the current density, however, was larger after immersion in BSA compared to immersion in deionized water for both sample types. Nevertheless, it was still possible to detect 100 µM H_2O_2 after immersion either in deionized water or BSA.

Table 3 summarizes the ΔE_p values for biofouling experiments with FcMeOH and changes in the peak positions and current densities for experiments with H_2O_2. In Table 3 positive $\Delta_{change}Ep$ denotes the peak has shifted in the positive direction whereas negative value marks peak shift in the opposite direction. DI water refers to deionized water.

3.4. Quartz crystal microbalance with dissipation monitoring (QCM-D)

The adsorption of BSA on ta-C, ta-C/Pt and Pt was further studied by QCM-D. The adsorbed mass of BSA, expressed as change in the resonance frequency of the crystal sensor, is presented in Figure 9. The initial baseline, corresponding to the situation where the substrates were in protein-free PBS buffer (pH ~7.4), is followed by a clear drop in frequency for all the samples when the BSA solution was injected into the system. A significant increase in mass uptake was observed for Pt compared to ta-C and ta-C/Pt at t = 20 min the adsorbed mass on Pt being 10% higher than that on the other two. Only about 5% of adsorbed BSA was washed away from all the surfaces when protein-free PBS was injected in the system, as revealed by the very small increase of frequency observed at t = 23 min in Figure 9.

In summary, QCM-D results indicate that BSA was adsorbed on all three sample types and could not be significantly washed away. This could also be seen from electrochemical experiments with FcMeOH in PBS (Figure 7) where all the samples were affected by immersion in BSA solution.

However, ta-C was not completely blocked like the other two sample types but exhibited clear peaks for FcMeOH oxidation and reduction. It is proposed to arise from different orientation of the protein on the surfaces. As the methods applied here do not give any information on protein orientation the proposition was not further verified and should be investigated in detail in the future.

QCM-D results are in line with those from the experiments conducted in PBS with H_2O_2 as the analyte (Figure 8). The hybrid sample (ta-C/Pt) fouls less in both experiments when compared to Pt. Interestingly, when experiments were carried out in acidic environment with FcMeOH (Figure 6) the hybrid sample was fouled significantly more than pure ta-C or pure Pt.

Thus, when planning biofouling studies on new materials it should be taken into account that protein (and electrode) behavior differs in different environments.

4. Conclusions

Pt containing hybrid ta-C samples were proposed to be suitable candidates for H_2O_2 detection. It was shown that addition of Pt in ta-C does not affect the conduction mechanism which remains as SCL current type. Both electrochemical and QCM-based biofouling experiments indicate that in neutral solutions the hybrid material suffers less from protein adsorption compared to pure Pt, which makes it feasible material for biosensor applications.

The optimal amount of Pt in the hybrid material still remains to be determined. Also, finding the most active orientation of Pt for H_2O_2 oxidation could improve the functionality of the sensor. In addition, the limit of detection and the range of linear response need to be investigated with the improved material.

It should be noted that the BSA solution utilized in biofouling experiments was very simple and does not represent the actual *in vivo* conditions. However, it is regarded as an adequate model as it gives some general guidelines for protein adsorption on the sample surfaces. In further studies more complex solutions should be used in order to obtain more detailed information.

Acknowledgements

The authors would like to acknowledge the Finnish Funding Agency for Technology and Innovation (TEKES), Academy of Finland, Biocentrum Helsinki, Finnish Concordia Fund, Tekniikan edistämissäätiö, and Aalto University for financial and technical support. E.K. received funding from the Academy of Finland grant #274670. V. P. would like to acknowledge Micronova Nanofabrication Centre and Department of Forest Products Technology for the provision of facilities and technical support. Sami Sainio and Iina Yrjänä are also acknowledged for their help in conducting the electrochemical experiments.

References

[1] A. J. Bard and L. R. Faulkner, *Electochemical methods: Fundamentals and Applications*, 2nd ed. Hoboken, NJ USA: Wiley and Sons, 2001, p. 864.

[2] A. M. Gómez-Marín, K. J. P. Schouten, M. T. M. Koper, and J. M. Feliu, Interaction of hydrogen peroxide with a Pt(111) electrode, *Electrochem. commun.*, vol. 22, pp. 153–156, 2012.

[3] A. Schneider, L. Colmenares, Y. E. Seidel, Z. Jusys, B. Wickman, B. Kasemo, and R. J. Behm, Transport effects in the oxygen reduction reaction on nanostructured, planar glassy carbon supported Pt/GC model electrodes, *Phys. Chem. Chem. Phys.*, vol. 10, pp. 1931–1943, 2008.

[4] M. Giorgio, M. Trinei, E. Migliaccio, and P. G. Pelicci, Hydrogen peroxide: a metabolic by-product or a common mediator of ageing signals?, *Nat. Rev. Mol. Cell Biol.*, vol. 8, pp. 722–728, 2007.

[5] Q. H. Gibson, B. E. P. Swoboda, and V. Massey, Kinetics and mechanism of action of glucose oxidase of action of glucose, *J. Biol. Chem.*, vol. 239, pp. 3927–3934, 1964.

[6] H. Kusakabe, Y. Midorikawa, T. Fujishima, A. Kuninaka, and H. Yoshino, Purification and properties of a new enzyme, L-glutamate oxidase, from Streptomyces sp. X-119-6 grown on wheat bran, *Agricultural and Biological Chemistry*, vol. 47, pp. 1323–1328, 1983.

[7] Q. K. Yue, I. J. Kass, N. S. Sampson, and A. Vrielink, Crystal structure determination of cholesterol oxidase from Streptomyces and structural characterization of key active site mutants, *Biochemistry*, vol. 38, pp. 4277–4286, 1999.

[8] R. L. McCreery, Advanced carbon electrode materials for molecular electrochemistry, *Chem. Rev.*, vol. 108, pp. 2646–2687, 2008.

[9] R. D. O'Neill, S.-C. Chang, J. P. Lowry, and C. J. McNeil, Comparisons of platinum, gold, palladium and glassy carbon as electrode materials in the design of biosensors for glutamate, *Biosens. Bioelectron.*, vol. 19, pp. 1521–1528, 2004.

[10] C. M. Welch, C. E. Banks, A. O. Simm, and R. G. Compton, Silver nanoparticle assemblies supported on glassy-carbon electrodes for the electro-analytical detection of hydrogen peroxide, *Anal. Bioanal. Chem.*, vol. 382, pp. 12–21, 2005.

[11] K. Cui, Y. Song, Y. Yao, Z. Huang, and L. Wang, A novel hydrogen peroxide sensor based on Ag nanoparticles electrodeposited on DNA-networks modified glassy carbon electrode, *Electrochem. commun.*, vol. 10, pp. 663–667, 2008.

[12] B. Zhao, Z. Liu, Z. Liu, G. Liu, Z. Li, J. Wang, and X. Dong, Silver microspheres for application as hydrogen peroxide sensor, *Electrochem. commun.*, vol. 11, pp. 1707–1710, 2009.

[13] P. Zhou, Z. Dai, M. Fang, X. Huang, J. Bao, and J. Gong, Novel dendritic palladium nanostructure and its application in biosensing, *J. Phys. Chem. C*, vol. 111, pp. 12609–12616, 2007.

[14] G. Nie, X. Lu, J. Lei, L. Yang, X. Bian, Y. Tong, and C. Wang, Sacrificial template-assisted fabrication of palladium hollow nanocubes and their application in electrochemical detection toward hydrogen peroxide, *Electrochim. Acta*, vol. 99, pp. 145–151, 2013.

[15] S. Hrapovic, Y. Liu, K. B. Male, and J. H. T. Luong, Electrochemical biosensing platforms using platinum nanoparticles and carbon nanotubes, *Anal. Chem.*, vol. 76, pp. 1083–1088, 2004.

[16] J. Wang, M. Musameh, and Y. Lin, Solubilization of carbon nanotubes by Nafion toward the preparation of amperometric biosensors, *J. Am. Chem. Soc.*, vol. 125, pp. 2408–2409, 2003.

[17] C. M. Welch and R. G. Compton, The use of nanoparticles in electroanalysis: a review, *Anal. Bioanal. Chem.*, vol. 384, pp. 601–619, 2006.

[18] N. Wisniewski and M. Reichert, Methods for reducing biosensor membrane biofouling, *Colloids Surfaces B Biointerfaces*, vol. 18, pp. 197–219, 2000.

[19] T. Goto, T. Yasukawa, K. Kanda, S. Matsui, and F. Mizutani, Inhibition of electrochemical fouling against biomolecules on a diamond-like carbon electrode, *Anal. Sci.*, vol. 27, pp. 91–94, 2011.

[20] W. Chen, S. Cai, Q.-Q. Ren, W. Wen, and Y.-D. Zhao, "Recent advances in electrochemical sensing for hydrogen peroxide: a review.," *Analyst*, vol. 137, pp. 49–58, 2012.

[21] S. B. Hall, E. A. Khudaish, and A. L. Hart, Electrochemical oxidation of hydrogen peroxide at platinum electrodes. Part II: effect of potential, *Electrochim. Acta*, vol. 43, pp. 2015–2024, 1998.

[22] T. J. Secker, R. Hervé, Q. Zhao, K. B. Borisenko, E. W. Abel, and C. W. Keevil, Doped diamond-like carbon coatings for surgical instruments reduce protein and prion-amyloid biofouling and improve subsequent cleaning, *Biofouling*, vol. 28, pp. 563–569, 2012.

[23] W. J. Ma, A. J. Ruys, R. S. Mason, P. J. Martin, A. Bendavid, Z. Liu, M. Ionescu, and H. Zreiqat, DLC coatings: effects of physical and chemical properties on biological response, *Biomaterials*, vol. 28, pp. 1620–1628, 2007.

[24] T. Laurila, V. Protopopova, S. Rhode, S. Sainio, T. Palomäki, M. Moram, J. M. Feliu, and J. Koskinen, New electrochemically improved tetrahedral amorphous carbon films for biological applications, *Diam. Relat. Mater.*, vol. 49, pp. 62–71, 2014.

[25] E. Kaivosoja, S. Sainio, J. Lyytinen, T. Palomäki, T. Laurila, S. I. Kim, J. G. Han, and J. Koskinen, Carbon thin films as electrode material in neural sensing, *Surf. Coatings Technol.*, vol. 259, pp. 33–38, 2014.

[26] N. Menegazzo, C. Jin, R. J. Narayan, and B. Mizaikoff, Compositional and electrochemical characterization of noble metal-diamondlike carbon nanocomposite thin films, *Langmuir*, vol. 23, pp. 6812–6818, 2007.

[27] M. L. Morrison, R. A. Buchanan, P. K. Liaw, C. J. Berry, R. L. Brigmon, L. Riester, H. Abernathy, C. Jin, and R. J. Narayan, Electrochemical and antimicrobial properties of diamondlike carbon-metal composite films, *Diam. Relat. Mater.*, vol. 15, pp. 138–146, 2006.

[28] Y. V. Pleskov, Y. E. Evstefeeva, and A. M. Baranov, Threshold effect of admixtures of platinum on the electrochemical activity of amorphous diamond-like carbon thin films, *Diam. Relat. Mater.*, vol. 11, pp. 1518–1522, 2002.

[29] E. Kaivosoja, N. Tujunen, V. Jokinen, V. Protopopova, S. Heinilehto, J. Koskinen, and T. Laurila, Glutamate detection by amino functionalized tetrahedral amorphous carbon surfaces, Unpublished results.

[30] E. Kaivosoja, E. Berg, A. Rautiainen, T. Palomäki, J. Koskinen, M. Paulasto-Kröckel, and T. Laurila, Improving the function of dopamine electrodes with novel carbon materials, *Proc. Annu. Int. Conf. IEEE Eng. Med. Biol. Soc. EMBS*, pp. 632–634, 2013.

[31] T. Laurila, A. Rautiainen, S. Sintonen, H. Jiang, E. Kaivosoja, and J. Koskinen, Diamond-like carbon (DLC) thin film bioelectrodes: effect of thermal post-treatments and the use of Ti adhesion layer, *Mater. Sci. Eng. C. Mater. Biol. Appl.*, vol. 34, pp. 446–454, 2014.

[32] G. Sauerbrey, “Verwendung von Schwingquarzen zur Wägung dünner Schichten und zur Mikrowägung,” *Zeitschrift für Phys.*, vol. 155, pp. 206–222, 1959.

[33] D.-Z. Guo, S.-M. Hou, G.-M. Zhang, and Z.-Q. Xue, Conductance fluctuation and degeneracy in nanocontact between a conductive AFM tip and a granular surface under small-load conditions, *Appl. Surf. Sci.*, vol. 252, pp. 5149–5157, 2006.

[34] H.-J. Butt, B. Cappella, and M. Kappl, Force measurements with the atomic force microscope: technique, interpretation and applications, *Surf. Sci. Rep.*, vol. 59, pp. 1–152, 2005.

[35] W. Frammelsberger, G. Benstetter, J. Kiely, and R. Stamp, C-AFM-based thickness determination of thin and ultra-thin SiO_2 films by use of different conductive-coated probe tips, *Appl. Surf. Sci.*, vol. 253, pp. 3615–3626, 2007.

[36] V. Protopopova, T. Laurila, S. Sainio, T. Palomäki, and J. Koskinen, Fabrication and electrical characterization of Ti/ta-C bilayers for biosensor applications, in *Abstracts of International conference on diamond and carbon materials*, 2014.

[37] P. W. May, M.-T. Kuo, and M. N. R. Ashfold, Field emission conduction mechanisms in chemical-vapour-deposited diamond and diamond-like carbon films, *Diam. Relat. Mater.*, vol. 8, pp. 1490–1495, 1999.

[38] J. Martinez-Vega, *Dielectric Materials for Electrical Engineering*. Hoboken, NJ USA: John Wiley & Sons, Inc., 2013.

[39] R. Purtell, G. Hollinger, G. W. Rubloff, and P. S. Ho, Schottky barrier formation at Pd, Pt, and Ni/Si(111) interfaces, *J. Vac. Sci. Technol. A Vacuum, Surfaces, Film.*, vol. 1, pp. 566–569, 1983.

[40] S. Sansongsiri, A. Anders, and B. Yotsombat, Electrical properties of a-C: Mo films produced by dual-cathode filtered cathodic arc plasma deposition, *Diam. Relat. Mater.*, vol. 17, pp. 2080–2083, 2008.

[41] J. Robertson, Diamond-like amorphous carbon, *Mater. Sci. Eng. R Reports*, vol. 37, pp. 129–281, 2002.

[42] A. C. Ferrari and J. Robertson, Raman spectroscopy of amorphous, nanostructured, diamond-like carbon, and nanodiamond., *Philos. Trans. A. Math. Phys. Eng. Sci.*, vol. 362, pp. 2477–2512, 2004.

[43] A. C. Ferrari and J. Robertson, Interpretation of Raman spectra of disordered and amorphous carbon, *Phys. Rev. B*, vol. 61, pp. 14095–14107, 2000.

[44] B. E. Conway, H. Angerstein-Kozlowska, W. B. A. Sharp, and E. E. Criddle, Ultrapurification of water for electrochemical and surface chemical work by catalytic pyrodistillation, *Anal. Chem.*, vol. 45, pp. 1331–1336, 1973.

[45] P. Delahay, Electrode Processes without a Priori Separation of Double-Layer Charging, *J. Phys. Chem.*, vol. 70, pp. 2373–2379, 1966.

[46] E. M. Hudak, J. T. Mortimer, and H. B. Martin, Platinum for neural stimulation: voltammetry considerations, *J. Neural Eng.*, vol. 7, 2010.

[47] S. B. Hall, E. A. Khudaish, and A. L. Hart, Electrochemical oxidation of hydrogen peroxide at platinum electrodes. Part V: inhibition by chloride, *Electrochim. Acta*, vol. 45, pp. 3573–3579, 2000.

[48] E. Sitta, A. M. Gómez-Marín, A. Aldaz, and J. M. Feliu, Electrocatalysis of H_2O_2 reduction/oxidation at model platinum surfaces, *Electrochem. commun.*, vol. 33, pp. 39–42, 2013.

[49] R. Gifford, J. J. Kehoe, S. L. Barnes, B. A. Kornilayev, M. A. Alterman, and G. S. Wilson, Protein interactions with subcutaneously implanted biosensors, *Biomaterials*, vol. 27, pp. 2587–2598, 2006.

[50] K. Chun and P. Stroeve, Protein Transport in Nanoporous Membranes Modified with Self-Assembled Monolayers of Functionalized Thiols, *Langmuir*, vol. 18, pp. 4653–4658, 2002.

[51] M. Vinnichenko, R. Gago, N. Huang, Y. X. Leng, H. Sun, U. Kreissig, M. P. Kulish, and M. F. Maitz, Spectroscopic ellipsometry investigation of amorphous carbon films with different sp^3 content: relation with protein adsorption, *Thin Solid Films*, vol. 455–456, pp. 530–534, 2004.

Figures

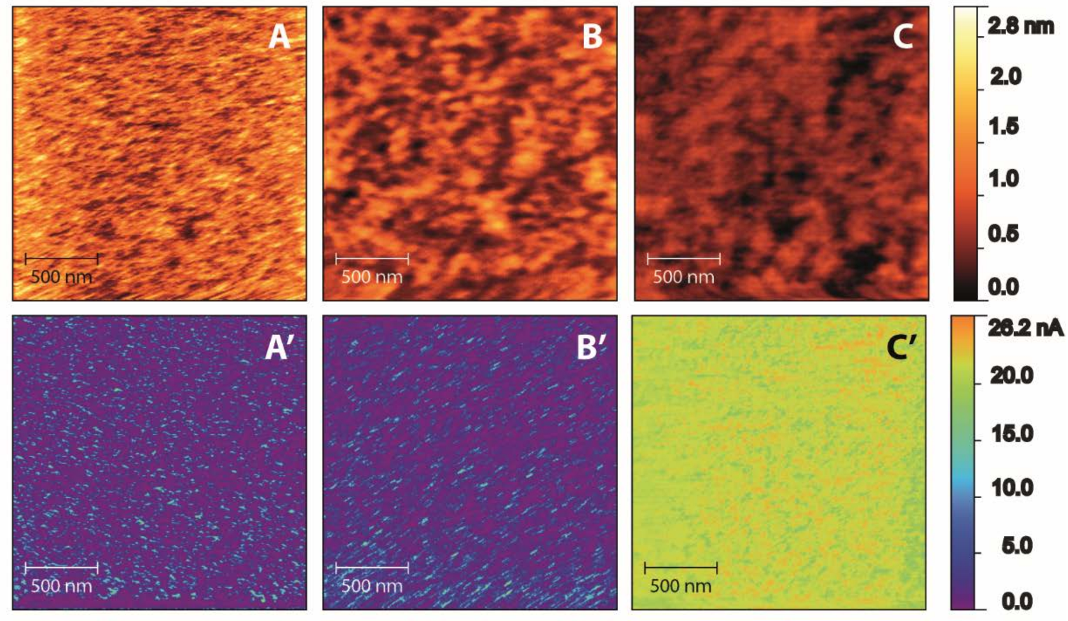

Figure 1. Topography (top row) and current (bottom row) maps for ta-C (A, A'), and ta-C/Pt (B, B') and Pt (C, C') samples. A' and B' current maps were obtained under 1 V of applied voltage, whereas C' current map was received under 0.1 V. HA_HP_DCP probe was used for all samples.

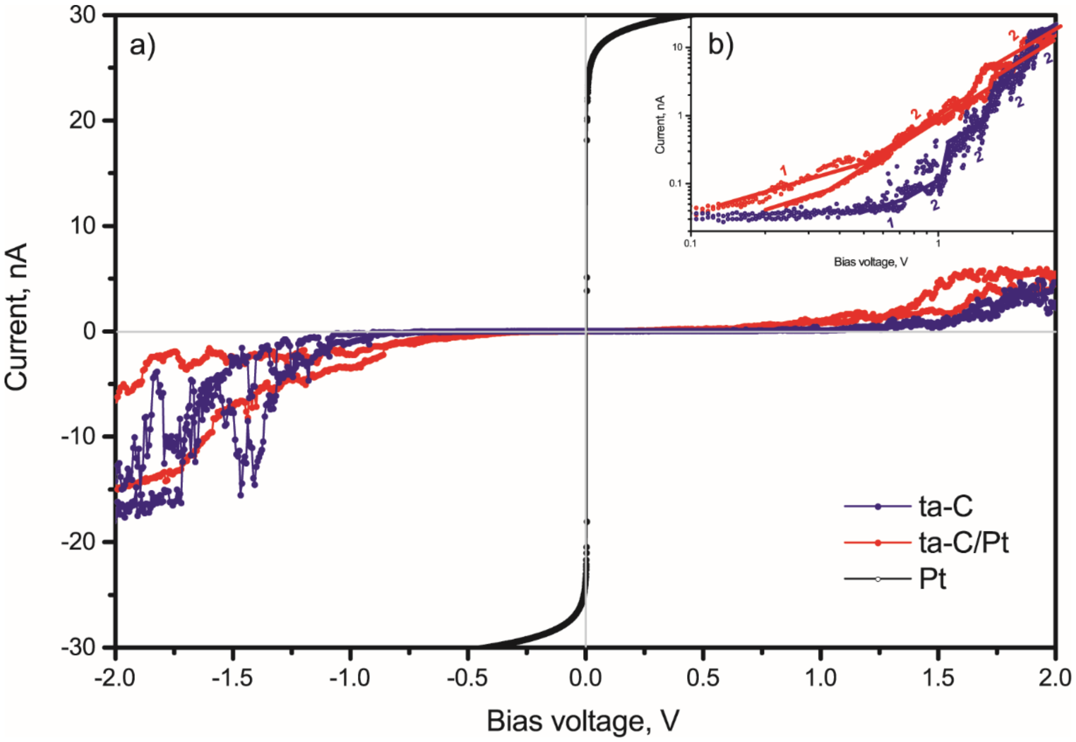

Figure 2. Current-voltage curves obtained from c-AFM measurements in a) linear and b) log-log coordinates. Numbers placed along the linear approximations in b) represent the slopes of the respective lines.

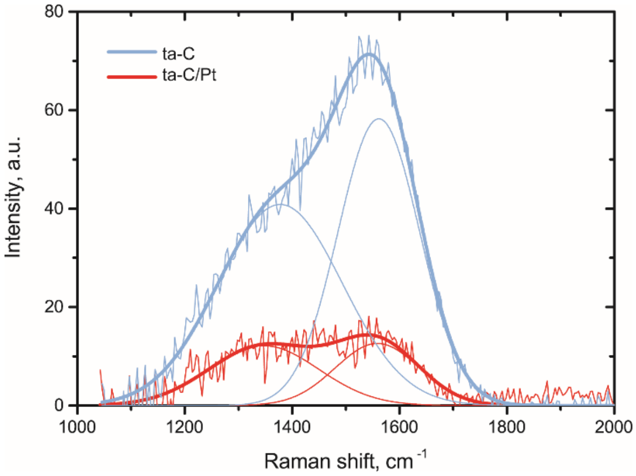

Figure 3. Raman spectra (background subtracted, no smoothing) of samples ta-C and ta-C/Pt.

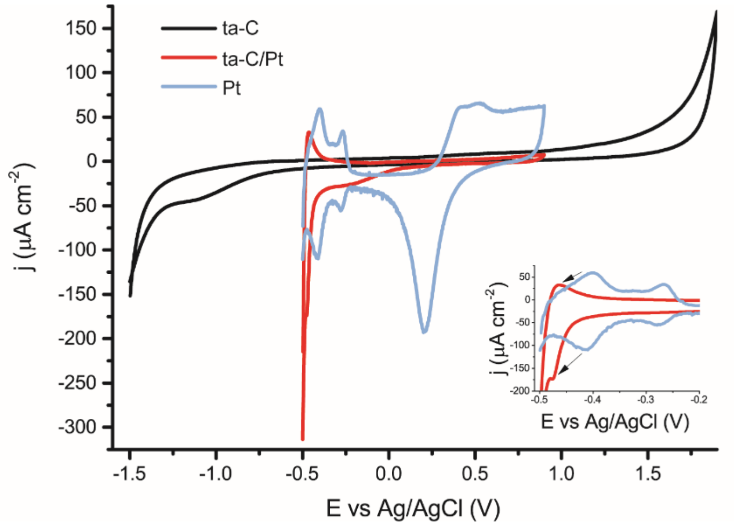

Figure 4. Voltammograms for samples ta-C, ta-C/Pt and Pt in 0.15 M H_2SO_4. The insets illustrate the proposed shifts in the hydrogen adsorption and desorption peaks for ta-C/Pt. Note that samples ta-C/Pt and Pt would allow cycling to higher potentials but here the range is limited in order to avoid any uncontrolled modification of Pt.

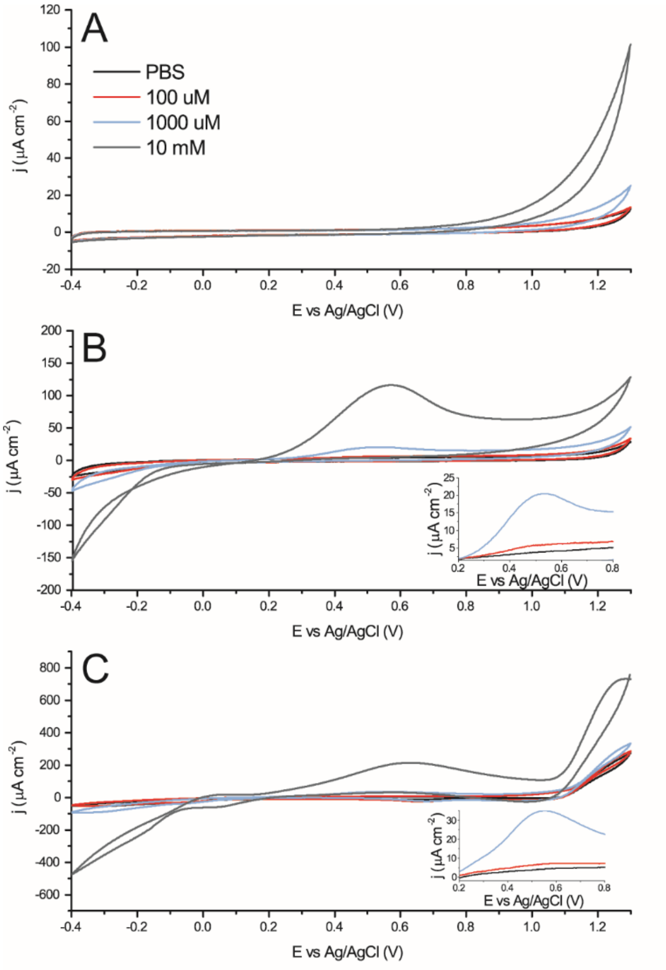

Figure 5. Cyclic voltammograms of pure ta-C sample (A), ta-C/Pt sample (B) and Pt sample (C) in 0-10 mM H_2O_2. The insets in B and C show the forward scans between 0.2V and 0.8 V for blank and 100 μM and 1000 μM H_2O_2 to illustrate the rise in the current with addition of the analyte.

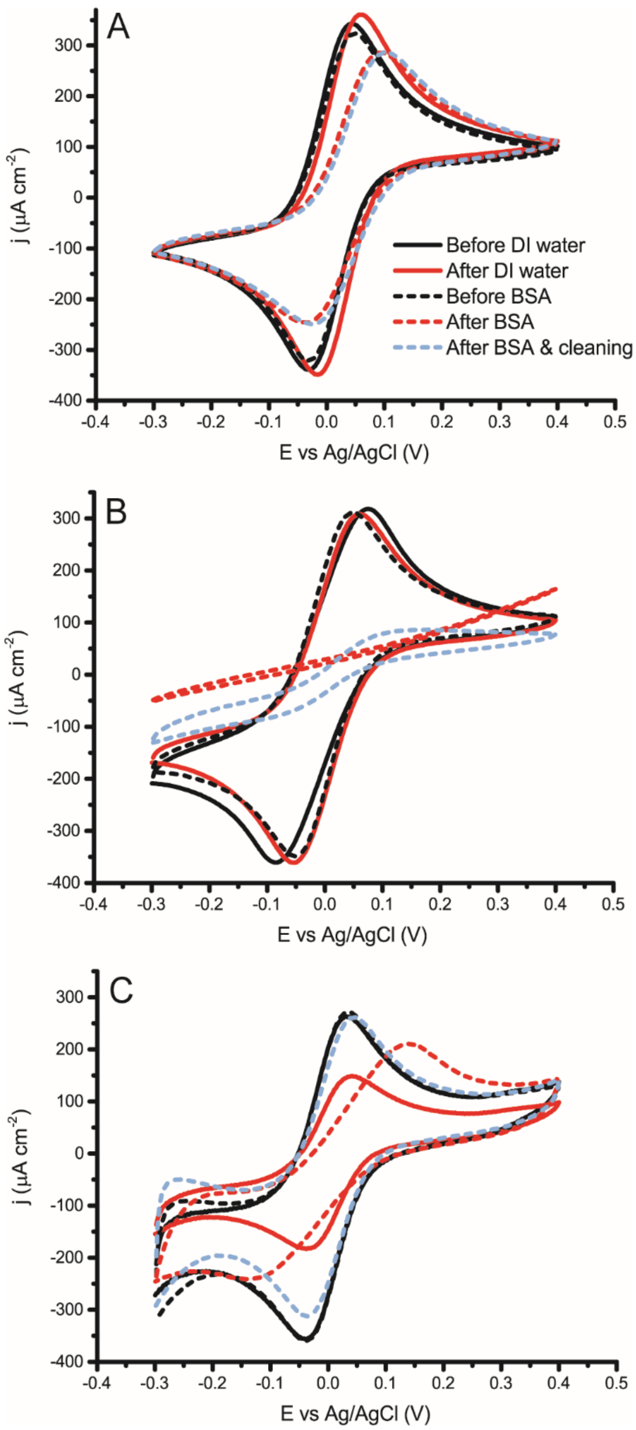

Figure 6. Responses for 1 mM FcMeOH in H2SO4 (pH < 1) for samples ta-C (A), ta-C/Pt (B) and Pt (C) before (black) and after (red) immersion in deionized water (solid lines) or 10 mg/ml BSA (dashed lines). Blue lines show the voltammograms after immersion and cleaning by cycling for 100 cycles in 0.15 M H_2SO_4.

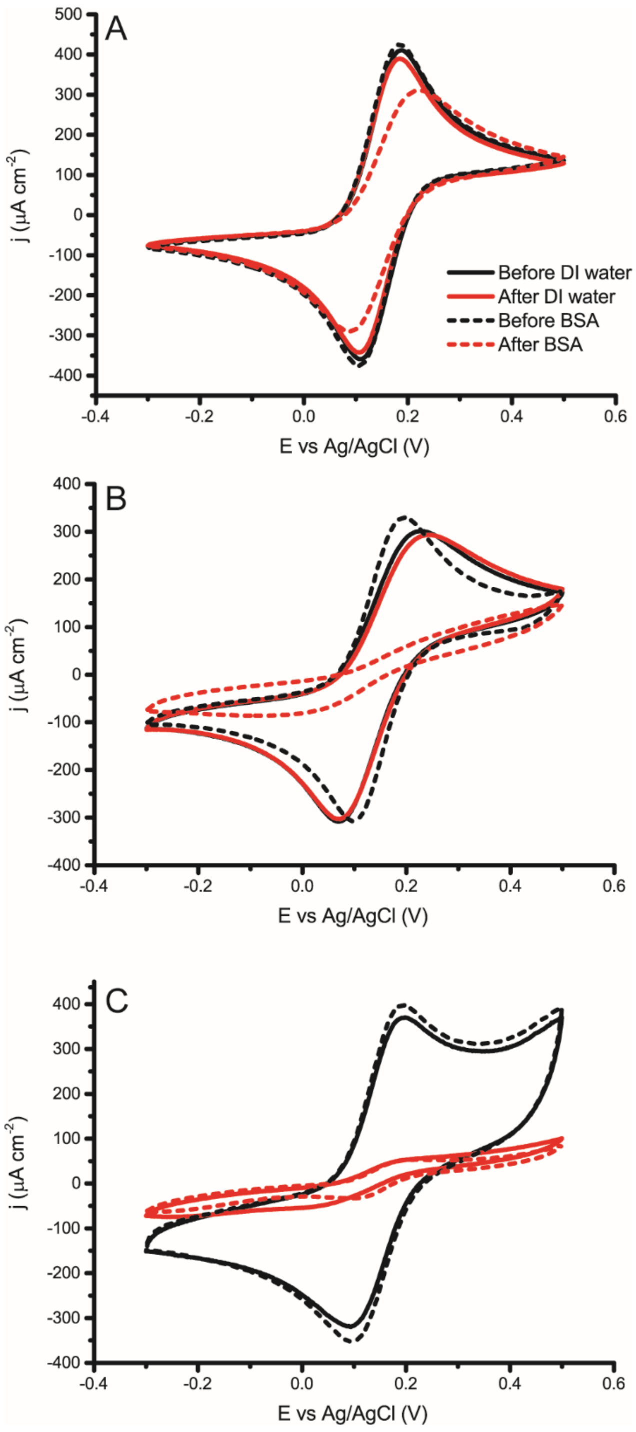

Figure 7. Responses for 1 mM FcMeOH in PBS (pH ~7.4) for samples ta-C (A), ta-C/Pt (B) and Pt (C) before (black) and after (red) immersion in deionized water (solid lines) or 10 mg/ml BSA (dashed lines).

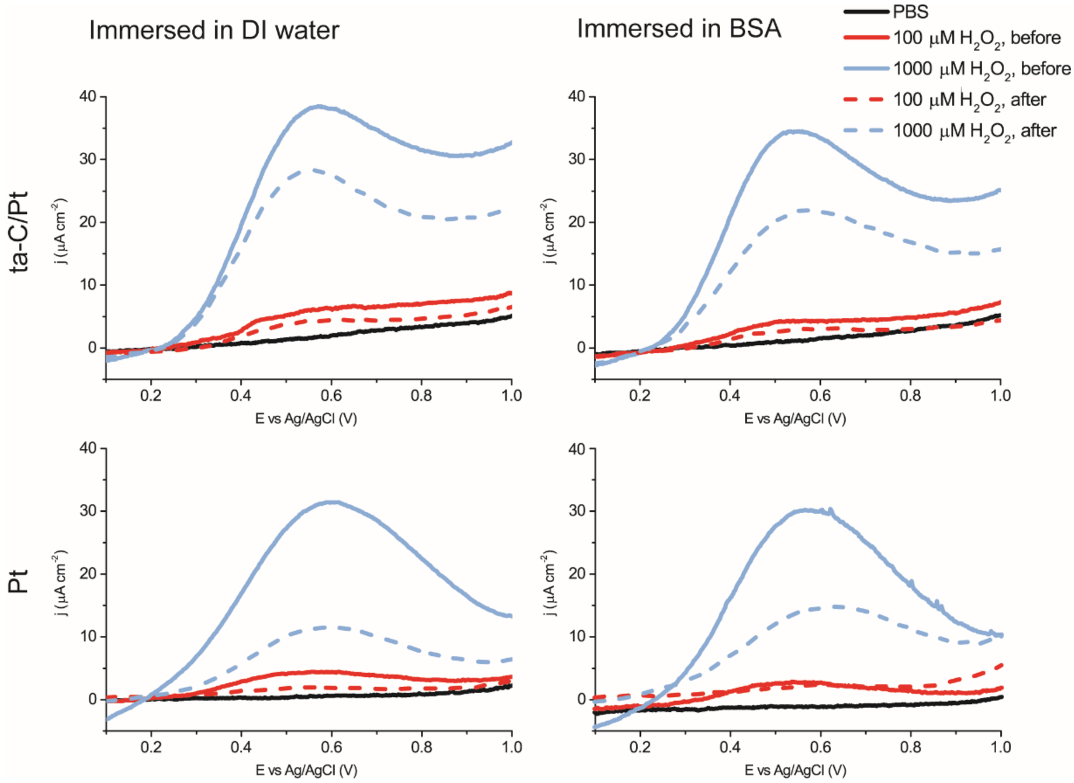

Figure 8. Responses to H_2O_2 for ta-C/Pt (top row) and Pt (bottom row) samples after immersion in deionized water (left) and 10 mg/ml BSA (right). DI water refers here to deionized water.

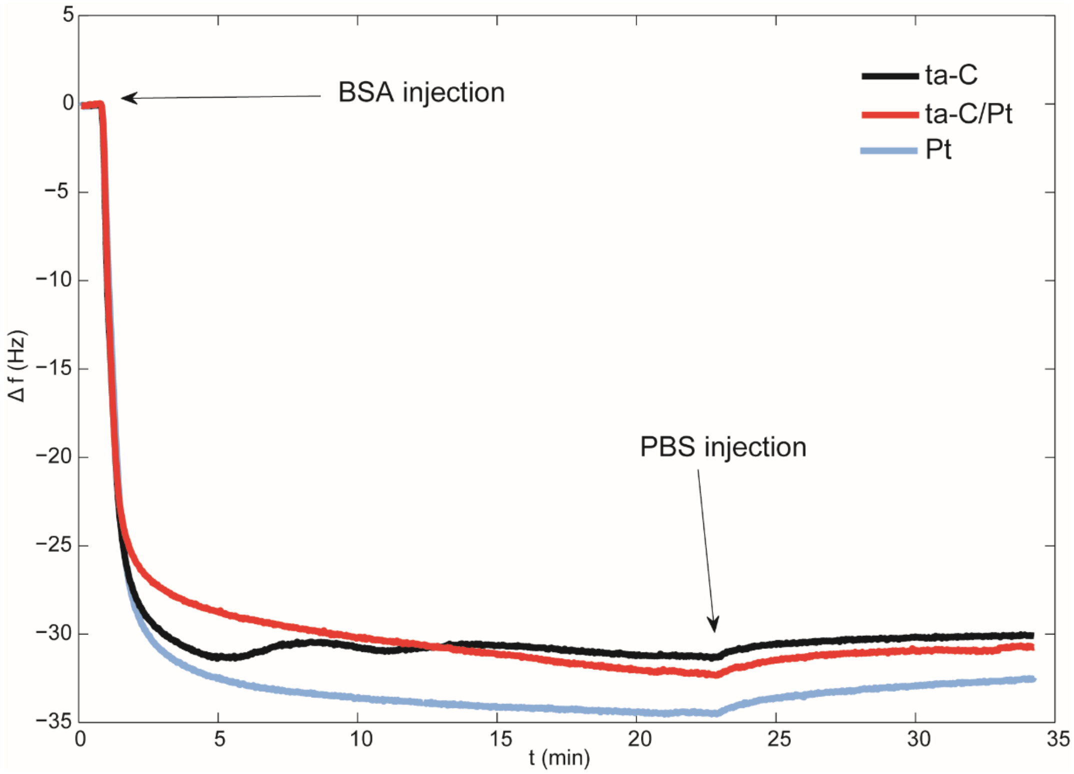

Figure 9. Adsorption of BSA on different surfaces expressed as change of the resonance frequency of QCM-D crystal sensors.

Tables

Table 1. Physical characteristics of studied samples. In cathode configuration representation (first row) black indicates carbon and grey Pt. Probe 1 and Probe 2 refer to DCP10 and HA_HP_DCP probes, respectively.

Sample	**ta-C**	**ta-C/Pt**	**Pt**
Cathode configuration representation	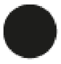		
C : Pt cathode area ratio, %	100 : 0	95 : 5	0 : 100
C : Pt atomic concentration, at. % (in film)	100 : 0	(80 : 20) ± 10	0 : 100
Layer structure of samples: · 20 nm Ti · 7 nm ta-C · 8 nm Pt	+ + –	+ + –	– – +
Roughness R_a, [nm]	1.15±0.14	1.08±0.28	0.43±0.11
Average current through samples [nA]: · Probe 1 · Probe 2	5.3 (at 0.3 V) 0.37 (at 1 V)	12.2 (at 0.3 V) 1.36 (at 1 V)	– 21.5 (at 0.1V)
Spreading resistance, [Ω cm] · Probe 1 · Probe 2	260 $8.9\cdot10^3$	95 $2.5\cdot10^3$	– 15.6
I(D)/I(G) ratio	0.7	0.96	–

Table 2. Summarized electrochemical characteristics for ta-C, ta-C/Pt and Pt samples.

Sample	**ta-C**	**ta-C/Pt**	**Pt**
Water window in H_2SO_4 (V)	3.5	1.8	1.8
Double-layer pseudocapacitance (0.15 M H_2SO_4) (μF cm^{-2})	44.8±13.4	29.8±5.7	51.0±25.5
ΔEp (FcMeOH, 400 mV/s) (mV) in H_2SO_4 in PBS	75 76	130 127	69 99
H_2O_2 (1 mM) E_p (mV)	-	536	554
H_2O_2 (1 mM) j_p (μA cm^{-2})		20.5	35.0

Table 3. FcMeOH oxidation and reduction peak separation for samples ta-C, ta-C/Pt and Pt (400 mV/s) and the change of peak position for 1000 uM H_2O_2 after immersion for samples B and C (50 mV/s).

Sample	**ta-C**		**ta-C/Pt**		**Pt**	
	DI water	**BSA**	**DI water**	**BSA**	**DI water**	**BSA**
ΔE_p FcMeOH in H_2SO_4(mV)	74	130	110	-	78	226
ΔE_p FcMeOH in H_2SO_4, cleaning (mV)		128				78
ΔE_p FcMeOH in PBS	78	136	170	-	-	-
$\Delta_{change}E_p$ H_2O_2 (1 mM) (mV)	-	-	-20.0	22.1	5.8	54.0
$\Delta_{change}j_p$ H_2O_2 (1 mM) (μA cm^{-2})	-	-	35.9	44.2	19.9	54.2